Carbon-Enhanced Photocatalysts with Dopamine Electronic Bridge Enriched in Adjustable Adsorption and Visible-Light Degradation for Multitasking Water Remediation

Yanchen Zhu, a Peng Fu, Linli Qin, Kun Liu, Junhao Li, Hao Ren, at and Xin Wang b,*

The integrated strategy using coupling photocatalysis and adsorption to treat liquid waste has attracted increased attention. In this work, a carbon enhanced photocatalyst (BiOBr@PSBM) with dopamine bridge was constructed using porous straw biochar (SBM) as loading carrier for efficient, multitasking water purification engineering, enhancing adjustable adsorption and visible-light degradation. A cellulose-targeted etching strategy was used to construct porous biochar carriers. Benefiting from the synergy of dopamine and carbon enhancement, the electron migration ability of composites enabled the heightened visible-light catalysis activities, and the efficient visible-light degradation (96.5%) for various dye pollutants was achieved. The optimized porous structure, amino-rich surface, and pH control adjustable surface charge properties endowed composites with multitasking ability. They achieved excellent and rapid capture Cr(VI) through static-dynamic adsorption (157.7 mg·g⁻¹, 40 min). The theoretical calculation with DFT framework was used to study the proposed adsorption-degradation mechanism and the degradation pathway of organic polluted molecules. Significantly, multiple recycling and environmental experiments indicated that photocatalysts boasted stable structure and regeneration, supporting their cost-effective and efficient remediation of wastewater containing various polluted species. This work provided a feasible strategy for developing advanced water purification materials by the utilization of low-value solid-waste.

DOI: 10.15376/biores.20.3.6218-6241

Keywords: Carbon enhanced photocatalyst; Cellulose-targeted etching; Porous biochar carriers; Visible-light degradation; Static-dynamic adsorption

Contact information: a: Jiangsu Provincial Key Lab of Sustainable Pulp and Paper Technology and Biomass Materials, College of Light Industry and Food Engineering, Nanjing Forestry University, Nanjing 210037, P. R. China; b: School of Light Industry and Engineering, Qilu University of Technology (Shandong Academy of Sciences), Shandong Academy of Sciences, Jinan 250353, China; *Corresponding authors: renhao@njfu.edu.cn (H. Ren); wangxinpolymer@qlu.edu.cn (X. Wang)

INTRODUCTION

Continuous discharge of industrial wastewater containing complex contaminants that are not able to be broken down during conventional wastewater treatment seriously harms the natural water environment (Bolisetty and Mezzenga 2016; Rojas and Horcajada 2020; Xiao et al. 2021; Almatouq et al. 2023). Owing to their high toxicity and non-biodegradability, this situation poses a high huge threat to ecosystems and human health (Suzuki et al. 2020; Ma et al. 2024; Repon et al. 2024). From these perspectives above, the strategies based on single systems are not adequate. Rather, a multitasking approach is

needed to overcome the persistence. More importantly, considering the cost of production, application and energy, the system should integrate simple and extended fabrication technology and the ability of the sustainable removal of various pollutants in water (Heck et al. 2019; Li et al. 2020b; Mai et al. 2021; Huang et al. 2022). By contrast, visible-light catalytic degradation driven by cleaner sunlight is desirable and shows economical, green, and universal advantages that operate to degrade the various organic pollutants (Li et al. 2022b; Liu et al. 2023; Kang et al. 2024). Despite such progress, challenges persist. The key is to fabricate material with high operation efficiency by simple design, thus achieving the advanced treatment of wastewater (Li et al. 2022a; Jia et al. 2023; Wang et al. 2023b). In addition, the multitasking capability of catalysts is required in terms of heterogeneous composition adaptability (Foong et al. 2022; Wang et al. 2023c). In this context, developing an advanced photocatalyst with multitasking application capabilities that response to this demand for the removal of complex pollutants is promising.

Photocatalysis based on clean sunlight has been demonstrated as an efficient and promising strategy for the advanced purification of wastewater, especially those containing organic pollutants, such as dyes (Sun et al. 2022; Peng et al. 2024; Ravindiran et al. 2024). Bismuth-based semiconductor photocatalysts (BiOBr) are suitable photocatalysis modules that are capable of the engineering of multitasking water purification materials (Zhu et al. 2021; Zhou et al. 2023; Zhang et al. 2024b), owing to their unique characteristics including unique spherical structure, appropriate band energy, and outstanding environmentally friendly. Unfortunately, single materials fabricated by monomers were generally limited by complex aqueous environment and limited light absorbance (Liu et al. 2019; Nothling et al. 2022; Wei et al. 2024). Thus, a non-destructive strategy is demanded to respond to this challenge involve simple and mild, effective process, enabling to significantly improve catalysis activity of materials at given low-cost condition. By comparison, highly efficient surface engineering based on dopamine (DA) mediated surface modification has been reported to improve the material properties, especially in catalytic ability (Chen et al. 2022; Li et al. 2025; Zhu et al. 2025). Interestingly, the surface-decorated polydopamine (PDA) can also serve as the electron transfer medium that enables the efficient carrier migration, in addition to enhancing adsorption (Wang et al. 2024; Zhang et al. 2024a). Their photothermal properties also positively contributed to trapping light and facilitating sanitizing photocatalysts (Wu et al. 2022; Saddique et al. 2023). As a result, an enhanced photocatalyst with highly efficient degradation ability dependent of light was facile developed.

With the characteristics of low-cost, biodegradable and rich-resources, plant-based biomass materials are important platform materials that build "green" functional materials (Li et al. 2020a; Zhao et al. 2020; Zhu et al. 2024). Notably, the authors have developed an efficient, low-cost and universal cellulose targeted etching strategy to prepare plant-based porous biomass materials (Guo et al. 2020). By utilizing this simple engineering design, the biobased carrier was conveniently constructed, which presents the optimized porous structure. Notably, the carbon-based carrier contributed to facilitating the electron transfer and thus sensitize the photocatalysts loaded on their surface (Senasu et al. 2021; Yang et al. 2022). In addition, the materials decorated by PDA coating showed amino-rich surface and pH control adjustable surface charge properties, enhances in interfacial capture, enabling the adsorption capacity. Abundant amino groups that serve as "adsorption tentacles" facilitated the capture of pollutants in water, enabling the multitasking application. Besides, the porous substrate also showed positive contribution to adsorption for pollutants. The porous structure and PDA coating can co-work for capturing pollutants

in water by adsorption. Thus, a synergistic effect of porous morphology and surface engineering was constructed to promote adsorption capability, enabling the multifunctional materials. Based on this, a composite with multitasking application ability that were able to remove different pollutants in adsorption and photodegradation process was easily constructed.

Motivated by the above, a multitasking composite biomass material (BiOBr/PSBM) was fabricated for multiple pollutants removal (Fig. 1a), enhanced adsorption capability, enhanced degradation performance, stable regeneration ability, and feasible scale-up preparation. Herbaceous waste was converted to biomass substrates with high porosity support for post-functionalization. The resulting PDA, which work as "organic heterojunction phases" contributed to the electron transfer of photocatalysts. Benefiting from those, the reported materials facilitated the removal of various pollutants involving heavy metal ions and organic polluted molecules. Significantly, the scalable preparation of such materials was desirable based on this simple and controllable synthesis process, suggesting its outstanding application ability.

EXPERIMENTAL

Materials and Chemicals

Straw material was obtained from a farm in Jiangsu province, China, and ground into powder (straw powder, SP, 40-60 mesh) by using a breaker. Lithium bromide (LiBr, 99%), dopamine (DA, 98%), and bismuth nitrate pentahydrate (Bi(NO₃)₃·5H₂O, 99.0%) were purchased from Energy Chemical Co., LTD, China. Sodium bromide (NaBr) and ethylene glycol (EG) were obtained from Macklin Co., LTD, China. Methylene blue (MEB) was purchased from Tianjin Chemical Reagent Research Co., LTD.

Synthesis of Porous Biochar Carrier

Firstly, SP was converted into the porous straw-biochar matrix (SBM). Specifically, 1 g of SP was added into 10 mL of LiBr (60 wt%) and kept at 120 °C for 2 h with a magnetic stirrer. In this process, the cellulose was removed from plant fibers. After the reaction, the crude samples were washed and dried to gain the porous SBM.

Fabrication of PDA-Modified SBM

Under magnetic stirring, 0.2 g of SBM and 50 mg of DA were successively dispersed in 50 mL of Tris buffer solution (pH=8.5). The mixed system was kept at 25 °C for 24 h to ensure sufficient decoration. The PDA modified SBM (PSBM) was obtained through purification with multiple deionized-water.

Synthesis of Carbon Enhanced Photocatalysts

By using the simple thermal synthesis, the composites were fabricated. In a typical synthesis process, 1 mmol of Bi (NO₃)₃·5H₂O and 1 mmol of NaBr were dissolved in 20 mL of EG, respectively. Then, 0.1 g of PSBM was added into Bi⁺-containing solution. The above two solution were stirred at 25 °C for 30 min. Subsequently, two suites of solution were mixed and further stirred for another 60 min. Then, the mixture was transferred to the reaction vessel (stainless autoclave) and kept at 160 °C for 6 h. After cooling, the targeted composites (BiOBr/PSBM) were obtained *via* washing and drying. In addition, BiOBr monomers were prepared using the same scheme for comparison.

Characterizations

The structure and application properties were characterized by using multiple characteristic methods, including Fourier Transform Infrared Spectra (FTIR, VERTEX 80V), X-ray photoelectron spectroscopy (XPS, AXIS UltraDLD), scanning electron microscope (SEM, Regulus 8100), and an electrochemical workstation (CHI 760E). The more detailed characterization descriptions were shown in Supporting Information S2.1 and S2.2.

Density Functional Theory (DFT)

To clarify the adsorption-degradation mechanism of materials and the possible degradation pathway of organic polluted molecules, the theoretical calculation with DFT framework of the reaction system was carried out using Materials Studio 2019. The orbital models of MEB and surface electrostatic potential of PDA were calculated.

Degradation Experiment

The MEB, as a widely used cationic (positively charged) organic dye in dyeing and printing industry, was selected to investigate the degradation capability of BiOBr/PSBM. The 10 mg of BiOBr/PSBM were dispersed into solution (C₀=50 mg/L, 20 mL) and stirred under sunlight. Each suite of experiments was performed three times. By controlling the solutional pH, the influence of environmental pH was investigated. The residual concentration in the solution was tested using a UV-vis spectrophotometer (Lambda 950, China), and the related degradation kinetic data were analyzed by using Eq. 1:

$$\ln\left(C_{t}/C_{0}\right) = -Kt\tag{1}$$

where C_t and C_0 (mg·L⁻¹) represent the measured concentration at different time and the initial concentration, respectively. K is the degradation rate constant.

Adsorption Experiments

The Cr(VI) valence state of chromium, which has high toxicity and is commonly found in industrial wastewater, was selected as the targeted heavy metal ion pollutant. By dissolving the K₂CrO₄ into acetate buffer solution, simulated Cr(VI)-containing wastewater was obtained. With a thermostatic shaker (240 rpm, 25 °C), the adsorption experiments were performed (10 mg of adsorbents added into 20 mL of Cr(VI)-containing wastewater) with threefold repetition. The used adsorbents were desorbed by adjusting pH and then sufficiently washed before repeated use to estimate the regeneration performance. Additionally, the effect of pH values (from 1.0 to 7.0) on adsorption capacity was further investigated. The ion concentration were traced by using an inductively coupled plasma optical emission spectrometer (ICP-OES, iCAPTM PRO XP, Thermo Scientific). The adsorption kinetic data were analyzed by using pseudo-first-order model (PFO, Eq. 2) and pseudo-second-order model (PSO, Eq. 3), as well as the Langmuir model (Eq. 4) and Freundlich model (Eq. 5) for adsorption isotherm data (Foo *et al.* 2010), as follows:

$$\ln (Q_{e} - Q_{t}) = \ln Q_{e} - K_{1}t \tag{2}$$

$$t/Q_t = t/Q_e + 1/(K_2Q_e^2)$$
(3)

where Q_e and Q_t (mg·g⁻¹) represent the adsorption amount at equilibrium time and test time, respectively. And K_1 (min⁻¹) and K_2 (g·mg⁻¹·min⁻¹) are the related adsorption rate constants.

$$C_{\rm e}/Q_{\rm e} = C_{\rm e}/Q_{\rm m} + 1/Q_{\rm m}K_{\rm L}$$
 (4)

$$lnQ_e = 1/nlnC_e + lnK_F$$
(5)

where Q_e and Q_m (mg·g⁻¹) represent the adsorption capacity at equilibrium time and the

maximum adsorption capacity in theory, respectively. C_e (mg·L⁻¹) is the remaining MEB concentration at equilibrium time. K_L (g·L⁻¹) and K_F (mg^{1-1/n}·L^{1/n}·g⁻¹) are the adsorbing rate constants of the above isotherm models.

RESULTS AND DISCUSSION

Structure Characterizations

The surface morphology of the sample was observed by SEM. The surface morphology of the composite material was changed in the course of the stepwise modifications. Compared with the straw with smooth surface (Fig. 1b), the SBM showed an open porous structure that contrasted strongly with the raw material (Fig. 1c). The hydrolysis of polysaccharide in biomass formed these porous structures characterized that featured high specific surface area characteristic. It was found that the BET test results were able to represent this change in a consistent manner. Figure 1d shows the SEM images of PSBM that operate with well-maintained porous structure after PDA decoration. Importantly, the PDA coating offered strong adhesion effect and thus established good interfacial compatibility between biomass substrate with BiOBr catalyst particles. After the in-situ synthesis, the shapely BiOBr particles were successfully immobilized on the surface of porous substrate to form the composites (Fig. 1e, Fig. S1). In addition, Fig. 1f shows the distribution of N, Bi, and Br elements. In general, there was a homogeneous distribution on the surface of BiOBr/PSBM, indicating the uniform decoration of PDA and immobilization of BiOBr.

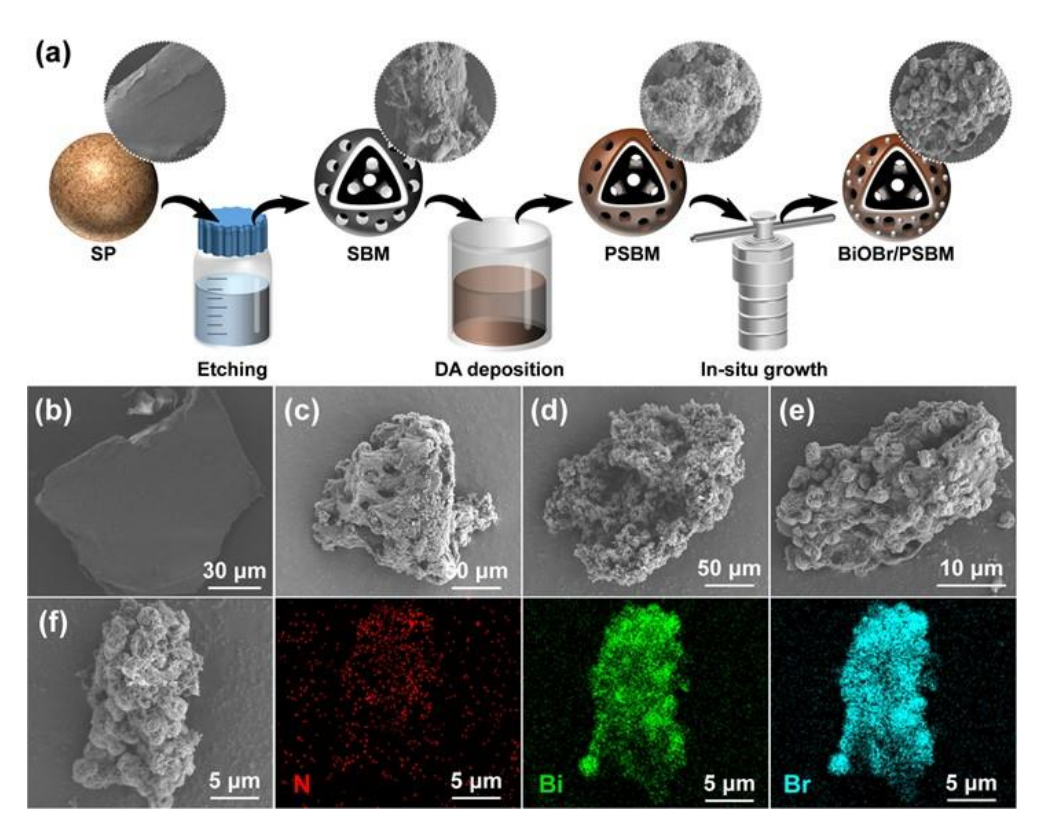


Fig. 1. (a) Schematic illustration of the synthesized BiOBr/PSBM. SEM images of samples: (b) Raw straw, (c) SBM, (d) PSBM, and (e) BiOBr/PSBM and (f) the SEM mapping images of BiOBr/PSBM

The chemical structures of the composite catalytic material were firstly confirmed by using FTIR spectra (Fig. 2a). Generally, the characteristic signal at 2911 cm⁻¹ was mainly attributed to the saturated C-H vibrations. Compared to straw, these characteristic signals in SBM, PSBM and BiOBr/PSBM were found to significantly decrease that due to the hydrolysis of polysaccharose (Guo et al. 2020). After the decoration of PDA, two typical adsorption peaks of PSBM appeared at 1608 and 1513 cm⁻¹, which could be assigned to the aromatic C=C resonance vibration and N-H bending vibration in the PDA coating, respectively (Zhang et al. 2021), thus indicating the successful modification of PDA coating. Through the in-situ growth of BiOBr, the catalysts particles were efficiently deposited on the biomass substrates, and the characteristic peak of Bi-O stretching vibration (518 cm⁻¹) was observed in the spectra of BiOBr/PSBM (Xu et al. 2023). The above results strongly suggested the fabrication of composite materials with rough reactive and degradation surface. The synthesis of BiOBr/PSBM was further verified via X-ray diffraction (XRD). As shown in Fig. 2b, BiOBr/PSBM spectrum displayed all typical diffraction peaks of BiOBr, inclusive of (101), (110), (200) and (212) crystal planes (JPDCS no. 09-0393) attributed to 25.1°, 32.5°, 46.2°, and 57.1° (Wen et al. 2022), strongly suggesting that in situ synthesis of BiOBr.

The N₂ adsorption-desorption tests was used to test the BET surface area (Fig. 2c). As suggested in a previous study (Guo *et al.* 2020), the etching strategy based on acid LiBr system facilitated constructing the biomass substrates with high porosity. After this treatment, SBM showed high specific surface area, as high as 34.0 m²·g⁻¹. After DA dipping and in-situ growth of BiOBr, BiOBr/PSBM presented higher specific surface area with a 1.18-fold increase, with 40.1 m²·g⁻¹, showing a well-maintained high specific surface area feature.

Table 1. BET Surface Area of Different Samples

Samples	Specific Surface Area (m²·g-¹)		
Straw	3.9		
SBM	34.0		
PSBM	26.6		
BiOBr/PSBM	40.1		

Further investigations of composite biomass materials were performed with XPS. As shown in Fig. 2d, the C, N, O, Bi and Br elements were observed in the full XPS spectra of BiOBr/PSBM, illustrating the successful fabrication of the composite. The C 1s could be divided into three peaks at 284.7 eV, 286.2 eV, and 288.6 eV (Fig. 2e), which corresponded to C-C, C-O, and C=O, respectively (Wu *et al.* 2024). The N 1s showed the presence of amino, inclusive of -NH₂ (399.7 eV) and -NH- (401.1 eV) (Fig. 2f). In O 1s spectrum, there were three peaks at 529.8 eV, 532.5 eV, and 533.7 eV (Fig. 2g) that correspond with Bi-O, oxygen vacancies, and chemical-absorbed oxygen (Wang *et al.* 2023a). The appearance of Bi 4f and Br 3d demonstrated the deposition of BiOBr (Fig. 2h and 2i) (Wang *et al.* 2023a). Due to the strong interfacial interaction between BiOBr and PDA coating, a binding energy shift movement phenomenon appeared. This suggested that the PDA operates as the electron transfer medium to support electron migration, thus avoiding the electron-hole recombination.

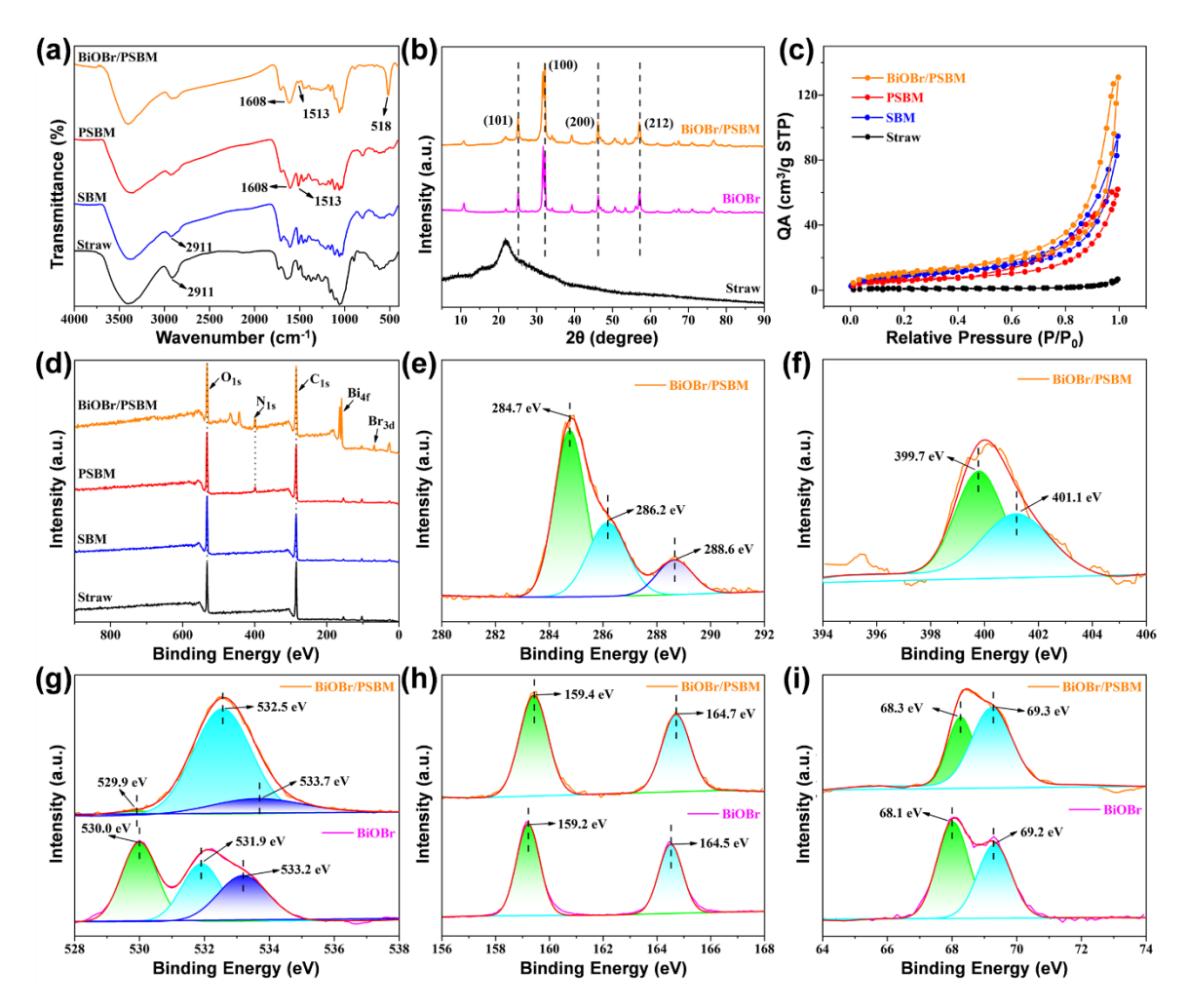


Fig. 2. The structure characterizations of BiOBr/PSBM: (a) FTIR spectra, (b) XRD spectra, (c) N₂ adsorption-desorption isotherms, (d) XPS full spectra, (e) C 1s spectra, (f) N 1s spectra, (g) O 1s spectra, (h) Bi 4f spectra, and (i) Br 3d spectra

Study on Optical and Photoelectrochemical Properties

The key is to realize excellent catalysis activity that operate systems with highly efficient light trapping and rapid electron transfer. The severe charge recombination and limited light absorbance of pure BiOBr makes their enhancement of catalysis activity challenging. Thus, there was only weak light absorbing in the case of pure BiOBr, showing that the absorbance edge only reached up to 462 nm (Fig. 3a). As expected, owing to the PDA modification and carbon enhancement, the BiOBr/PSBM exhibited a significant improvement in light absorbing efficiency. It was thereby able to capture a broad-spectrum of light on a wide range of spectra. Furthermore, the bandgap energies of them were investigated by using the related equation (Eq. 6),

$$E_{\rm g} = hv - (\alpha hv/A)^{2/n} \tag{6}$$

where A is a constant, α is the absorption coefficient, h is the Planck constant, v represents the light frequency. Through calculation, the bandgap energies of BiOBr and BiOBr/PSBM were 2.68 and 1.14 eV, respectively (Fig. 3b). The results demonstrated that BiOBr/PSBM showed narrower bandgap energy, which confirmed the efficient light absorption capability. This indicated that the reported BiOBr/PSBM more easily adsorbed sunlight

and then sensitized. The color changes of samples were provided as consistent evidence that supported the efficient light adsorbing capability (Fig. 3c).

Lower fluorescence intensity means faster separation rate of electron-hole pairs (Bera et al. 2024; Ji et al. 2024). The electron transfer efficiency of BiOBr/PSBM was investigated in terms of PL tests. As shown in test results (Fig. 3d), the BiOBr/PSBM showed a strong decrease in fluorescence intensity compared to other samples, suggesting a highly efficient separation efficiency of electron-hole pairs of it. This benefited from the loading of PDA that are able to induce the electron rapid migration. In addition, the electron transfer efficiency of BiOBr/PSBM was further indicated through the photocurrent response tests. This test result indicated that the BiOBr/PSBM presented a significantly high electron migration efficiency compared to BiOBr monomer (Fig. 3e). Furthermore, the electrochemical impedance spectroscopy (EIS) tests also observed that BiOBr/PSBM showed a smaller circular radius, supporting this rapid electron transfer performance (Fig. 3f). As a result, the electron migration kinetics were significantly enhanced. The effect was driven by the synergy of PDA electron bridge and carbon enhancement, which suggested a superior photodegradation capability for organic pollutants in water based on the reported carbon enhanced photocatalysts.

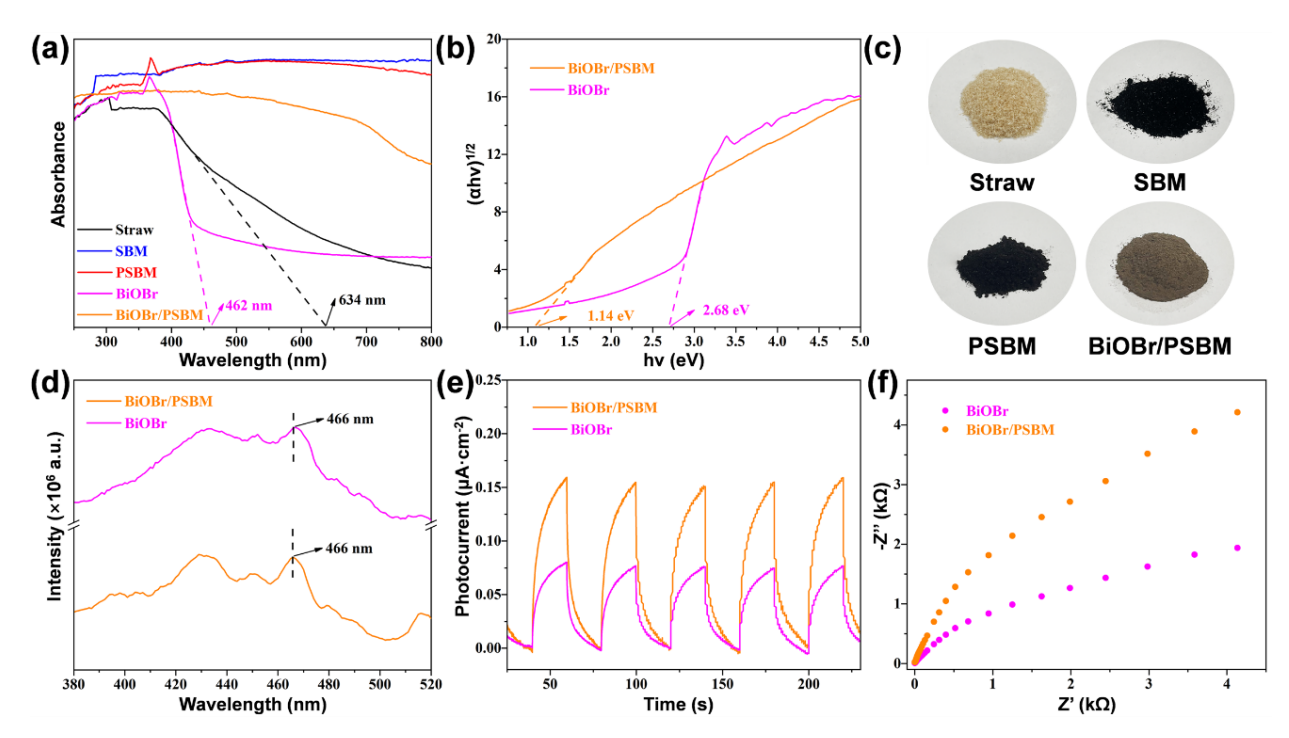


Fig. 3. (a) UV-vis DRS absorption spectra, (b) bandgaps energy, and (c) digital image of different samples. The electrochemical properties of BiOBr/PSBM: (d) PL spectra, (e) photocurrent response curves, and (f) EIS curves

Photodegradation Performance of BiOBr/PSBM

Organic dyes are diverse. Many of them have high toxicity, complex composition, and very slow or impossible biodegradation, such that it is difficult to achieve effective treatment. In particular, non-biodegradation is the best damaged for water security. Therefore, the typical organic dye, Methylene blue (MEB), was selected to verify the photodegradation of the reported BiOBr/PSBM composites. Benefiting from the introduction of PDA-sensitized and carbon enhanced BiOBr catalysis microspheres, the

BiOBr/PSBM exhibited excellent degradation efficiency (96.5%) for MEB compared to single BiOBr system or carbon enhancement system, its degradation was improved by 3.2 and 20.1 times, respectively, in comparison to the other two systems (Fig. 4a-b). The application efficiency of BiOBr/PSBM in various use amounts was measured, and the degradation capability was clearly positively correlated with use amount (Fig. 4c). Expanding to various dye pollutants, such photocatalyst also showed efficient removal efficiency (Fig. S2). These results indicated the synthesized BiOBr/PSBM was an efficient purification material support for the removal of organic pollutants in water. Notably, the BiOBr/PSBM still showed a stable and high degradation efficiency through repeated use (≥90% of degradation efficiency after 5 cycles), showing a stable regeneration and recycle performance (Fig. 4d). By using XRD spectra, their structure stability was confirmed. The result showed a similar crystal structure contained no significant change with fresh samples, demonstrating the stable structure of BiOBr/PSBM (Fig. S3). Benefiting from the advantages above, the disposal of dye-containing wastewater on the industrial scale was judged to be feasible by scalable preparing BiOBr/PSBM.

The degradation mechanism was tested through free radicals trapping experiments (Supporting Information S2.3). Isopropanol (IPA), ethylene diamine tetraacetic acid (EDTA-2Na), and benzoquinone (BQ) were used to capture ·OH, holes and ·O2 radicals. In the absence of trapping reagents, a high degradation efficiency of 96.5% was confirmed, while the degradation efficiency for organic dye pollutants was significantly decreased with the addition of trapping reagents (Fig. 4e), with 34.0, 71.6, and 76.6% decrease, respectively. This change was due to the decrease in available radicals in the degradation system, resulting in a weak degradation efficiency. Thereinto, EDTA and BQ showed obvious influence in degradation efficiency, indicating that photogenerated holes and ·O2 were the main active species that operate in the degradation process.

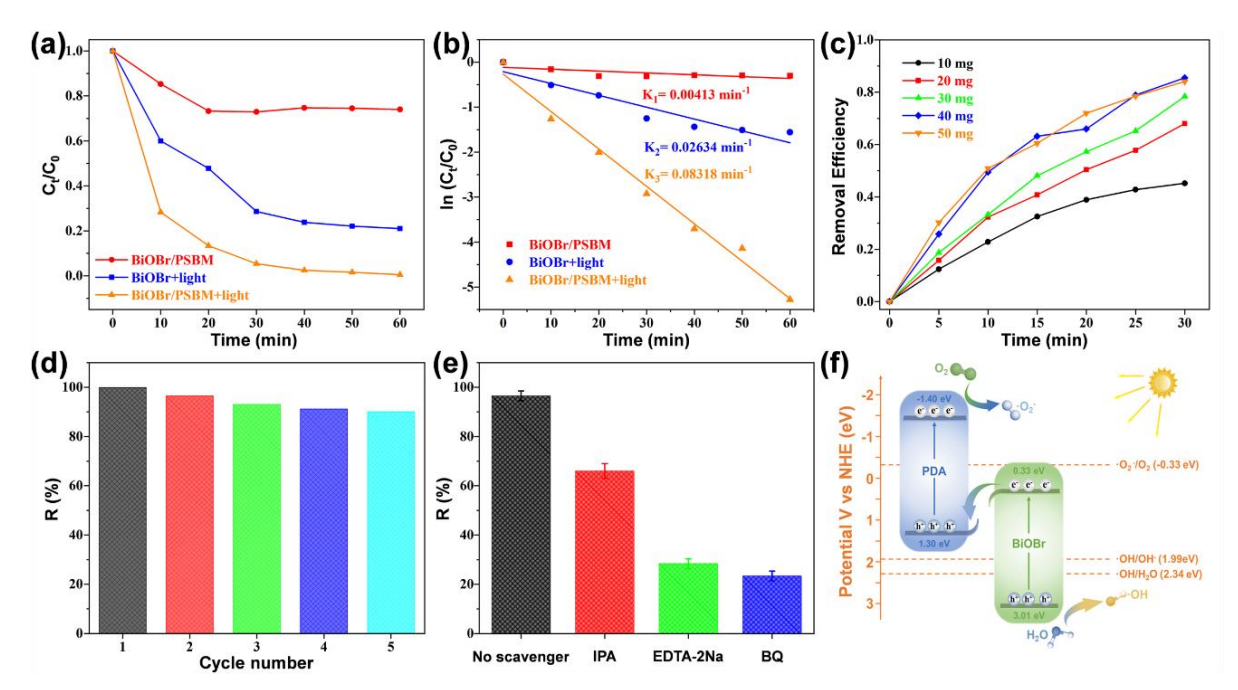


Fig. 4. (a) The degradation curves and (b) the related degradation rate of different system. (c) The effect of additive amount of BiOBr/PSBM. (d) The regeneration performance of BiOBr/PSBM. (e) The degradation efficiency under different trapping reagents. (f) The proposed electron transfer pathway on BiOBr/PSBM

Based on the results shown above and calculated bandgap distribution (Supporting Information S2.4), the proposed degradation mechanism of BiOBr/PSBM for organic dye were confirmed. The calculated E_{VB} and E_{CB} of BiOBr were 3.01 and 0.33 eV respectively. In addition, PDA showed similar VB and CB (HOMO and LUMO), which was calculated as 1.30 eV and -1.4 eV, respectively. Thus, a "heterojunction-like" structure was constructed between BiOBr and PDA. After light irradiation, the electron was excited from the VB_{BiOBr} and then transferred to CB_{BiOBr}. At this time, the hole (h⁺) was simultaneously formed in VB_{BiOBr}, which can directly attack the organic pollutants in wastewater. With the "heterojunction-like" structure, the excited electrons were transferred by PDA into environment and finally captured by free O₂ to form the \cdot O₂. Additionally, the OH⁻/H₂O in water can be oxidized by the strong oxidizing h⁺ to form \cdot OH. Those radicals can cowork to degrade the organic pollutants in wastewater. Based on those analyses, the proposed electron transfer pathway on BiOBr/PSBM was confirmed (Fig. 4f). The formed free radicals can efficiently degrade the captured organic pollutants to a small molecular harmless substance, thus achieving the effective purification of dye-containing wastewater.

The degradation reaction complexity makes the analysis of specific degradation pathway of model pollutants due to various reaction channels with multi-steps. As shown in Fig. 5, the possible degradation pathways of MEB model pollutants were explored by considering the GC-MS test results and DFT theoretical calculation (Fig. S4, Fig. S5). The DFT theoretical calculation results demonstrated that the high electron density was mainly concentrated around the -NH= group, while the low electron density region was mainly concentrated around the amino group at both ends. Combining with Fukui index, the =Sand -NH= groups in the middle of the benzene ring of MEB were considered as the reaction site prior attacked by electrophilic active substances (·O₂-) owing to the unsaturated bonds, as well as the terminal amino groups. After then, the benzene ring structure was further dissociated by nucleophilic active substances (h⁺) and finally formed the harmless inorganic substances (including CO₂, H₂O, NO₃ and SO₄²). This showed that major reactions in degradation process mainly included sulfur/nitrogen breaking or oxidation, and aromatic ring breaking. Based on this, the harmful organic dyes were degraded into harmless products by the reported BiOBr/PSBM photocatalysts, enabling the purification of dye-containing industrial wastewater.

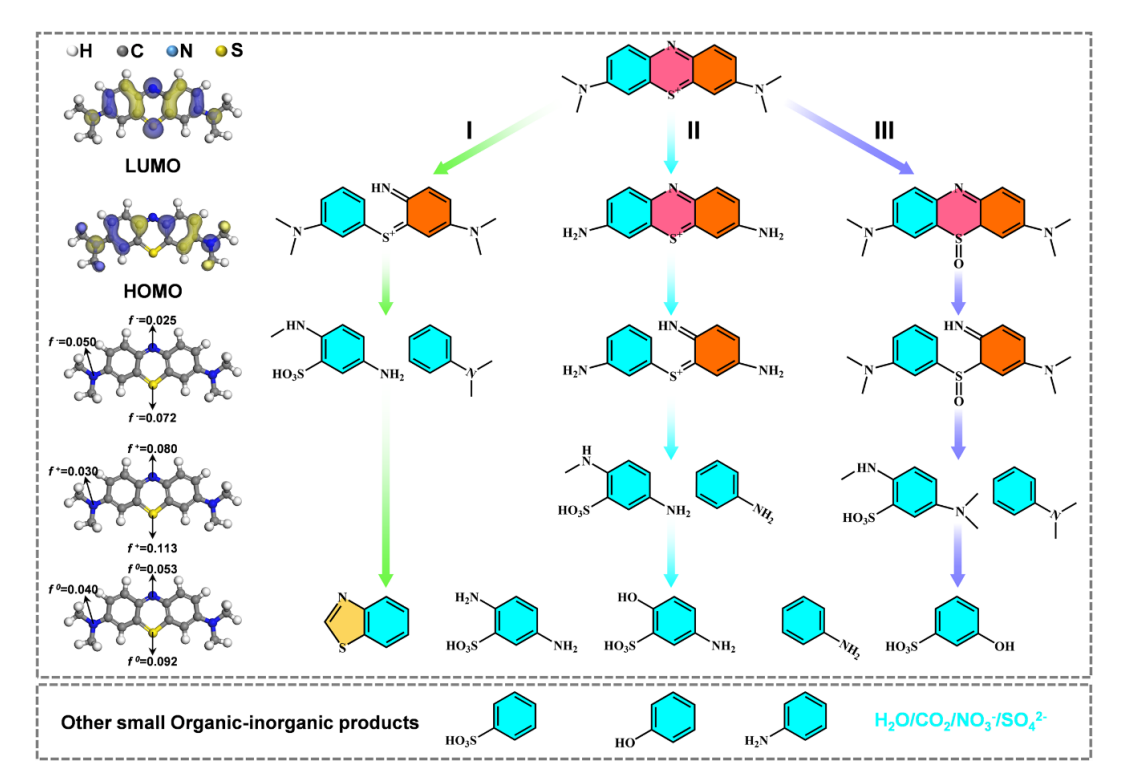


Fig. 5. The possible degradation pathways of MEB model pollutants

Multitasking Application of BiOBr/PSBM for Water Purification

Taking advantage of porous structure and amino-rich coating, the reported BiOBr/PSBM showed multitasking application ability. Serving as biochar-based adsorbents, this material was able to capture the various pollutants, such as heavy metal ions, at low cost. As expected, the designed BiOBr/PSBM presented significantly increased adsorption capability for Cr(VI) than straw, porous SBM carrier and PDA decorated PSBM, the adsorption capacity was reached up to 185.5 mg·g⁻¹ (Fig. 6a), indicating the suggested high adsorption capability of BiOBr/PSBM.

Adsorption systems prepared at different pH values were used to investigate the adsorption mechanism for Cr(VI). The results indicated an obvious negative relation between adsorption capacity and pH values that enables decreased adsorption at increased pH values, confirming a pH-dependent feature (Fig. 6b). The zeta potential at different environment pH was tested (Fig. 6c) to further give an insightful explanation about adsorption mechanism. As shown in Fig. 6c, the pH point of isoelectric charge (pHic) was between pH 5.0 and pH 6.0. It is easily seen that the surface potential charge became positive at decreased pH (pH<pH_{ic}) due to the protonation of amino groups, as well as negative of surface potential charge at high pH environment (pH>pHic) due to the deprotonation of them. Thus, a strong electronic interaction between protonated -NH₃⁺/-NH₂⁺- and HCrO₄⁻ was generated that was offered an efficient adsorption driven force for the capture of Cr(VI) at a given low pH condition. When the pH increased, the surface electrical properties of BiOBr/PSBM were significantly changed to negative, and instead the weak adsorption capability. As a result, the proposed adsorption mechanism on BiOBr/PSBM was confirmed (Fig. 3d) by combining the above analysis. Benefiting from this pH-dependent adsorption-desorption characteristics, the stable reusability of BiOBr/PSBM was realized by a simple adjustment of the pH values (Fig. 6e). Notably, driven by catalytic process, the highly toxic Cr(VI) was reduced into nontoxic Cr(III), which provided a "second way" for the removal of Cr(VI) (Fig. S6). This enabled the feasible application of the reported materials that can serve as the advanced and cost-effective adsorbents for the purification of real wastewater.

Another key to being considered as advanced adsorbents is facile integration with simple and stable water purification infrastructures. By using self-building filtering column loading the reported photocatalysts, the flowing purifying performance of BiOBr/PSBM was investigated (Fig. 6f). As shown in Fig. 6g, the BiOBr/PSBM showed stable and high removal capability (>70%) for a large volume of Cr(VI) by dynamic operation strategy, exhibiting a dynamic adsorption ability. This ability was conducted by the optimized structure and the enrichment of surface amino groups. Significantly, by scale-preparing the fabricated materials, the large-scale purification of industrial wastewater can be easily achieved. Additionally, the optimal operation was further surveyed through adjusting the feed rate and initial concentration of solution (Fig. 6h). The results demonstrated that lower feed rate and solution concentration facilitated the filtering removal of Cr(VI). The high feed rate resulted in insufficient capture time, as well as premature reach of saturated adsorption capacity at given high solution initial concentration. As a result, the key is to realize the optimal process that adjusts feed rate and initial concentration of solution. Those investigations further supported the applicability of BiOBr/PSBM that are able to serve as the advanced and cost-effective adsorbents.

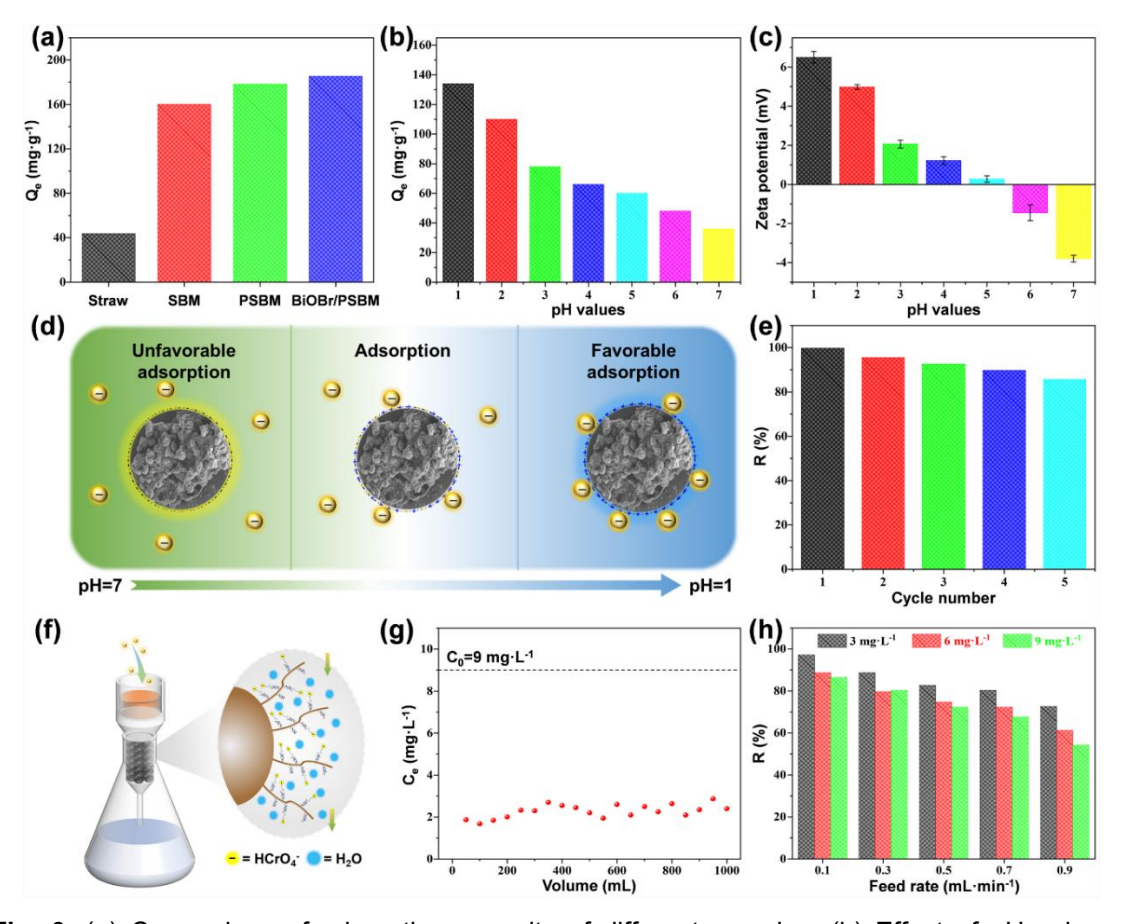


Fig. 6. (a) Comparison of adsorption capacity of different samples. (b) Effect of pH value on adsorption capability. (c) Surface zeta potential at different pH. (d) Proposed adsorption mechanism on BiOBr/PSBM. (e) Reusability of BiOBr/PSBM. (f) Schematic illustration of flowing removal infrastructures loading BiOBr/PSBM. (g) Continuous removal capability of a large volume of Cr(VI)-containing wastewater. (h) Effect of feed rate and initial concentration for removal capability

Study of the Adsorption Mechanism based on DFT

Based on the theoretical calculation with DFT framework, the adsorption-degradation mechanism of BiOBr/PSBM was investigated. The surface electrostatic potential (SEP) distributions of the models are shown in Fig. 7a-c. The SEP of Cr(VI) model showed obvious negative properties due to their existing form (HCrO4⁻) in the acidic environment (Fig. 7a). When the system was in an acidic condition, the SEP near the amino group of PDA showed significant positive properties, which was attributed to the protonation of amino groups at given pH=1.0 condition (Fig. 7b). As a result, a strong electrostatic attraction forms between them that enabled the capture of Cr(VI). When the pH changed to near-neutral condition, the SEP of materials changed fundamentally, and the electrostatic interaction transferred into a weak interaction (Fig. 7c). Fortunately, the porous structure of carbon reinforcements endowed composites with a certain adsorption capability at given facts, regardless of whether there were the interface interactions between the two (Fig. 7d). Thus, the adsorption-desorption attachment mechanism on BiOBr/PSBM was further determined by reasonable theoretical calculation based on DFT.

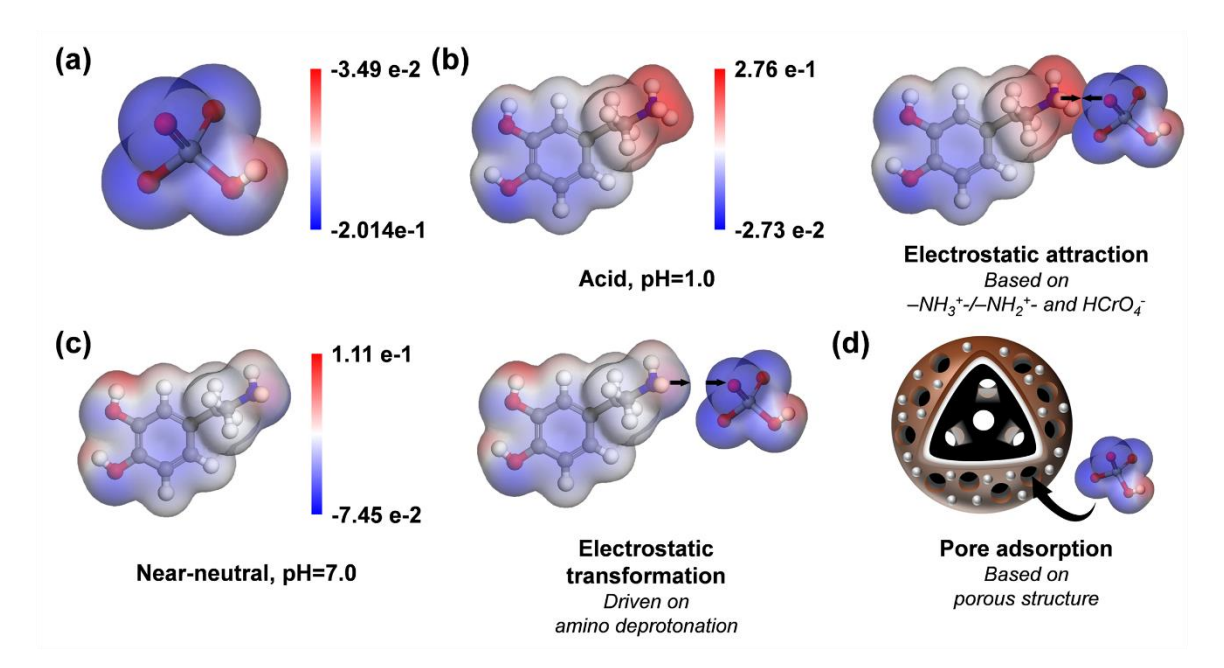


Fig. 7. The DFT calculations: (a) The Cr(VI) models and their surface electrostatic potential. (b, c) The calculated electrostatic potential of PDA and the proposed adsorption mechanisms for Cr(VI). (d) The pore adsorption on BiOBr/PSBM

Study on Adsorption Behavior

The adsorption behavior of BiOBr/PSBM was investigated in terms of different interval times and initial concentrations. For adsorption kinetics, the Cr(VI) adsorption on BiOBr/PSBM reached the equilibrium state within 50 min, exhibiting a quick adsorption process (Fig. 8a). By using PFO model and PSO model, the kinetic data were fitted. The relevant fitting results are summarized in Table 2. As the results show, the PSO model presented a well-fitting consistency compared to the PFO model (Fig. 8b, Fig. S7a). This chemical driven force was derived by amino-rich coating, which facilitated capturing Cr(VI).

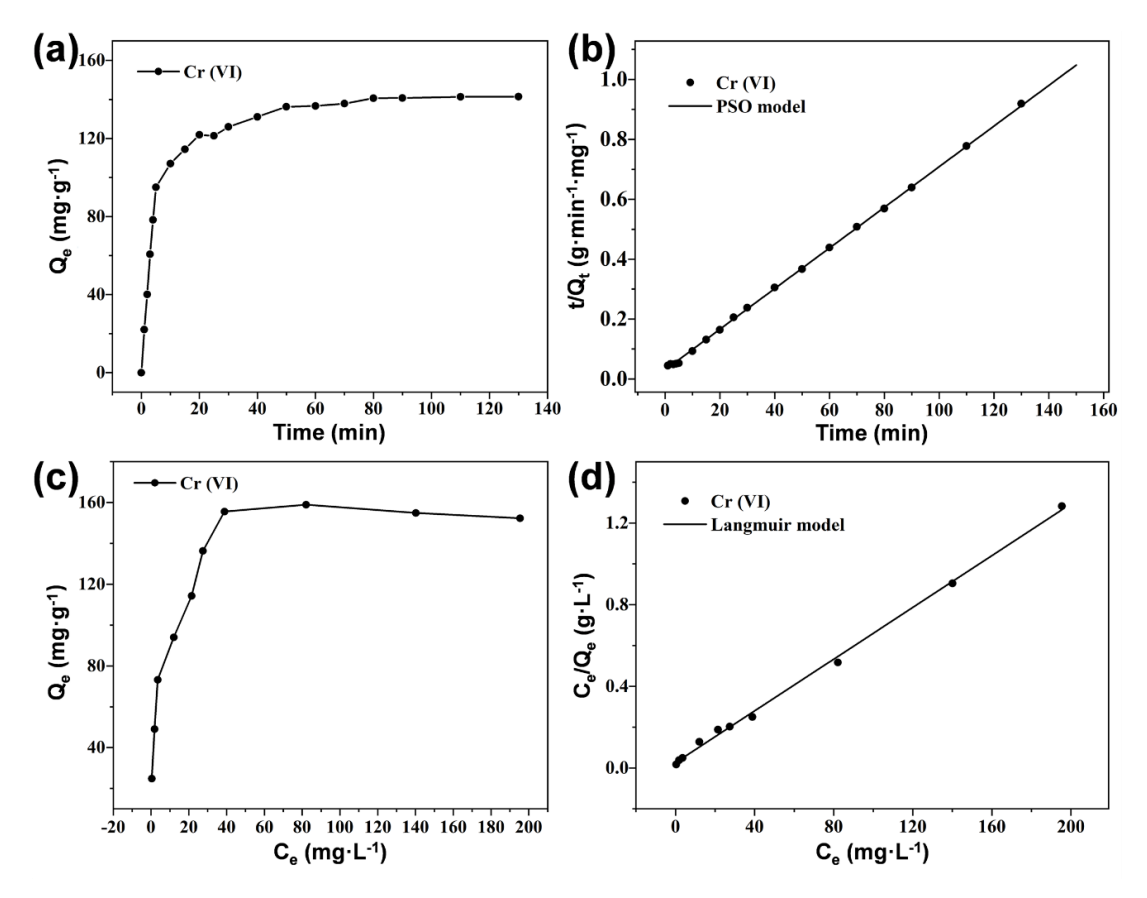


Fig. 8. (a) Adsorption kinetic curves of Cr(VI) on BiOBr/PSBM and (b) corresponding PSO model fitting results. (c) Adsorption isotherm curves and (d) corresponding Langmuir model fitting results.

Table 2. Kinetic Fitted Parameter for Cr (VI) Adsorption

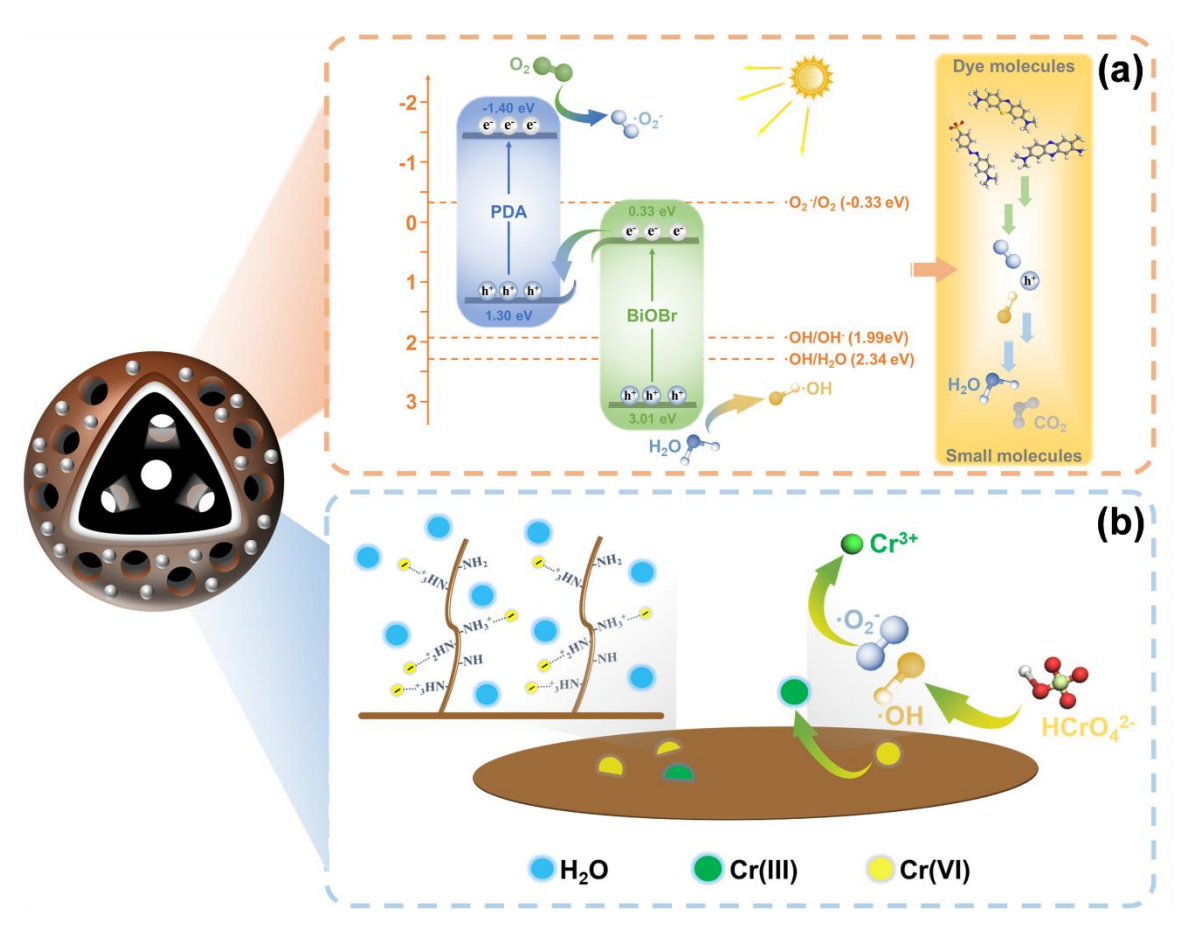
Metal ion	Model	Fitted Parameters		
Cr (VI)	PSO	R^2	Q _e (mg⋅g ⁻¹)	K_2 (g·mg ⁻¹ ·min ⁻¹)
		0.9996	147.5	1.5E-3
	PFO	R^2	Q _e (mg⋅g ⁻¹)	<i>K</i> ₁ (min⁻¹)
		0.8767	65.0	3.1E-2

The adsorption isotherm experiments were performed by adjusting the initial concentrations of Cr(VI) to further evaluate the adsorption behavior. The results indicated that the adsorption capacity of BiOBr/PSBM was increased at given increased initial concentrations of solution, and it gradually reached adsorption saturation (Fig. 8c). The isothermal data were analyzed through Langmuir and Freundlich models. The fitting results are summarized in Table 2. According to the fitting results, the Langmuir model showed a higher fitting goodness (Fig. 8d, Fig. S7b) than the Freundlich model. This result demonstrated a monolayer adsorption process with no interaction between adjacent sites (Chen *et al.* 2018; Xu *et al.* 2020). Thus, a monolayer chemisorption behavior on BiOBr/PSBM was confirmed. Combining with the kinetics fitting results, a monolayer chemisorption process was confirmed. The surface amino-rich coating contributed to improving the interfacial contact between liquid and solid that enabled the efficient capture and removal of Cr(VI) at assist of porous structure. By calculation, the saturation of Cr(VI) was 157.7 mg·g⁻¹, theoretically.

Metal ion	Model	Fitted Parameters		
Cr(VI)	Langmuir	R ²	Q _m (mg⋅g ⁻¹)	<i>K</i> ∟ (g·L ⁻¹)
		0.9977	157.7	4.1
	Freundlich	R ²	n	K _F (mg ^{1-1/n} ·L ^{1/n} ·g ⁻¹)
		0.8998	3.4	42.0

Table 3. Isotherm Fitted Parameter for Cr(VI) Adsorption

Significantly, the reported carbon-enhanced photocatalyst (BiOBr@PSBM) with dopamine bridge incorporated a simple fabrication process and feasible extended preparation, enriching in efficient visible-light degradation and excellent adsorption. Benefiting from this, the developed composites can be used to treat larger volumes containing various pollutants (Scheme 1) and supports the purification of larger scalable industrial wastewater.



Scheme 1. The pollutants pathways on BiOBr/PSM: (a) photodegradation for organic pollutants, (b) adsorption for heavy metal ions

CONCLUSIONS

1. An innovative design of polydopamine (PDA) electron bridge loading carbonenhanced photocatalyst, BiOBr/PSBM, was fabricated based on low-cost biochar carriers, which was enriched in efficient light degradation of organic dyes, as well as adjustable adsorbed Cr(VI) in water. In this synthesis, a mild and reliable cellulose

- targeted removal strategy was used to construct the biochar carriers with high porosity. Benefiting from the synergy of PDA and carbon enhancement, the electron migration ability of composites enabled the high visible light catalysis activities, and the efficient visible-light degradation (96.5%) for various dye pollutants was achieved.
- 2. The optimized porous structure, amino-rich surface, and pH control adjustable surface charge properties endowed composites with excellent adsorption capability (157.7 mg·g⁻¹), rapid adsorption process (40 min), and adjustable adsorption feature.
- 3. The theoretical calculation with density functional theory (DFT) framework provided insightful study of the proposed adsorption-degradation mechanism and the degradation pathway of organic polluted molecules.
- 4. Notably, multiple recycling and environment experiments revealed the reported photocatalysts boasted stable structure and regeneration, which supports the cost-effective and efficient remediation of wastewater containing various polluted species.
- 5. This work developed an advanced and cost-effective carbon enhanced photocatalyst by utilizing agriculture solid waste. This research provides new insights into the simultaneous removal of multiple pollutants in polluted water.

ACKNOWLEDGMENTS

This work was funded by the National Key Research and Development Program of China [grant numbers 2017YFD0601005].

CONFLICT OF INTEREST

The authors declare there is no conflict of interest regarding the publication of this paper.

REFERENCES CITED

- Almatouq, A., Ahmed, M. E., Khajah, M., Abdullah, H., Al-Yaseen, R., Al-Jumaa, M., Al-Ajeel, F., and Shishter, A. (2023). "Performance of tubular microbial fuel cells using different industrial wastewater," *Journal of Water Process Engineering* 55, article 104166. DOI: 10.1016/j.jwpe.2023.104166
- Bera, D., Mahata, S., Biswas, M., Kumari, K., Rakshit, S., Nonappa, Ghosh, S., and Goswami, N. (2024). "Efficient photocatalytic hydrogen production using *in-situ* polymerized gold nanocluster assemblies," *Small*, article 2406551. DOI: 10.1002/smll.202406551
- Bolisetty, S., and Mezzenga, R. (2016). "Amyloid-carbon hybrid membranes for universal water purification," *Nature Nanotechnology* 11, 365-371. DOI: 10.1038/NNANO.2015.310
- Chen, Y., Lu, K. J., Liang, C. Z., and Chung, T. S. (2022). "Mechanically strong Janus tribore hollow fiber membranes with asymmetric pores for anti-wetting and anti-fouling membrane distillation," *Chemical Engineering Journal* 429, article 132455. DOI: 10.1016/j.cej.2021.132455
- Foo, K. Y., and Hameed, B. H. (2010). "Insights into the modeling of adsorption

- isotherm systems," *Chemical Engineering Journal* 156, article 2-10. DOI: 10.1016/j.cej.2009.09.013
- Foong, S. Y., Chan, Y. H., Chin, B. L. F., Lock, S. S. M., Yee, C. Y., Yiin, C. L., Peng, W., and Lam, S. S. (2022). "Production of biochar from rice straw and its application for wastewater remediation An overview," *Bioresource Technology* 360, article 127588. DOI: 10.1016/j.biortech.2022.127588
- Guo, F., Chen, J., Zhao, J., Chen, Z., Xia, D., Zhan, Z., and Wang, Q. (2020). "Z-scheme heterojunction g-C₃N₄@PDA/BiOBr with biomimetic polydopamine as electron transfer mediators for enhanced visible-light driven degradation of sulfamethoxazole," *Chemical Engineering Journal* 386, article 124014. DOI: 10.1016/j.cej.2020.124014
- Heck, K. N., Garcia-Segura, S., Westerhoff, P., and Wong, M. S. (2019). "Catalytic converters for water treatment," *Accounts of Chemical Research* 52, article 906-915. DOI: 10.1021/acs.accounts.8b00642
- Huang, S., Wang, Y., Wan, J., Yan, Z., Ma, Y., Zhang, G., and Wang, S. (2022). "Ti₃C₂T_x as electron-hole transfer mediators to enhance AgBr/BiOBr Z heterojunction photocatalytic for the degradation of tetrabromobisphenol A: Mechanism insight," *Applied Catalysis B: Environmental* 319, article 121913. DOI: 10.1016/j.apcatb.2022.121913
- Ji, X., Liu, Y., Gao, Z., Lin, H., Xu, X., Zhang, Y., Zhu, K., Zhang, Y., Sun, H., and Duan, J. (2024). "Efficiency and mechanism of adsorption for imidacloprid removal from water by Fe-Mg co-modified water hyacinth-based biochar: Batch adsorption, fixed-bed adsorption, and DFT calculation," Separation and Purification Technology 330, article 125235. DOI: 10.1016/j.seppur.2023.125235
- Jia, S., Wu, Y., Zhou, H., Yan, H., Liao, Y., and Mao, H. (2023). "Plant tannin foam anchored iron nanoparticles: Efficient and recyclable degradation of tetracycline antibiotics under high salt conditions," *Journal of Cleaner Production* 426, article 139188. DOI: 10.1016/j.jclepro.2023.139188
- Kang, K., Li, R., Wang, S., Huang, Z., and Li, J. (2024). "Adsorption sites and interactions of pigments in molasses-based distillery effluent on starch-based composites: Ternary competitive adsorption and theoretical calculations," *Journal of Hazardous Materials* 480, article 136137. DOI: 10.1016/j.jhazmat.2024.136137
- Li, G., Zeng, G., Tang, N., Lu, L., Li, M., Yu, J., Long, W., Hu, X., Tan, X., and Tang, C. (2025). "Floatable expanded perlite-loaded Z-scheme n-C₃N₅/Ag₂CO₃ core-shell structure with C-defects for enhanced adsorption and photodegradation of microcystin-LR: Insights into performance and mechanism," *Applied Catalysis B: Environment and Energy* 361, article 124614. DOI: 10.1016/j.apcatb.2024.124614
- Li, J., Yuan, H., Zhang, W., Jin, B., Feng, Q., Huang, J., and Jiao, Z. (2022). "Advances in Z-scheme semiconductor photocatalysts for the photoelectrochemical applications: A review," *Carbon Energy* 4, article 294-331. DOI: 10.1002/cey2.179
- Li, X., Yu, Z., Shao, L., Zeng, H., Liu, Y., and Feng, X. (2020). "A novel strategy to construct a visible-light-driven Z-scheme (ZnAl-LDH with active phase/g-C₃N₄) heterojunction catalyst via polydopamine bridge (a similar "bridge" structure)," *Journal of Hazardous Materials* 386, article 121650. DOI: 10.1016/j.jhazmat.2019.121650
- Li, Y. X., Shen, J. X., Peng, S. S., Zhang, J. K., Wu, J., Liu, X. Q., and Sun, L.-B. (2020). "Enhancing oxidation resistance of Cu(I) by tailoring microenvironment in zeolites for efficient adsorptive desulfurization," *Nature Communications* 11, article 3206.

- DOI: 10.1038/s41467-020-17042-6
- Li, Z., Wang, X., Kuang, W., Dong, C., Fan, Y., Guo, Y., Qiao, Q., Zhu, Z., Liu, Y., and Zhu, Y. (2022). "Biofiber waste derived zwitterionic and photocatalytic dye adsorbent: Switchable selectivity, in-situ degradation and multi-tasking application," *Bioresource Technology* 352, article 127080. DOI: 10.1016/j.biortech.2022.127080
- Liu, Y., Wang, X., and Feng, S. (2019). "Nonflammable and magnetic sponge decorated with polydimethylsiloxane brush for multitasking and highly efficient oil-water separation," *Advanced Functional Materials* 29, article 1902488. DOI: 10.1002/adfm.201902488
- Liu, Z., Ma, Z., Pang, X., Ahmad, M., Zhao, Y., Su, N., Liu, J., Zhang, Y., Sun, H., Subhan, F., and Yan, Z. (2023). "Electrospinning prepared nickel-based carbon fibers with enhanced adsorption capacity for adsorption desulfurization of fuels," *Chemical Engineering Journal* 478, article 147254. DOI: 10.1016/j.cej.2023.147254
- Ma, H., Yu, L., Yang, L., Yao, Y., Shen, G., Wang, Y., Li, B., Meng, J., Miao, M., and Zhi, C. (2024). "Graphene oxide composites for dye removal in textile, printing and dyeing wastewaters: A review," *Environmental Chemistry Letters* 23, article 165-193. DOI: 10.1007/s10311-024-01794-4
- Mai, H., Chen, D., Tachibana, Y., Suzuki, H., Abe, R., and Caruso, R. A. (2021). "Developing sustainable, high-performance perovskites in photocatalysis: Design strategies and applications," *Chemical Society Reviews* 50, article 13692-13729. DOI: 10.1039/d1cs00684c
- Nothling, M. D., Bailey, C. G., Fillbrook, L. L., Wang, G., Gao, Y., McCamey, D. R., Monfared, M., Wong, S., Beves, J. E., and Stenzel, M. H. (2022). "Polymer grafting to polydopamine free radicals for universal surface functionalization," *Journal of the American Chemical Society* 144, article 6992-7000. DOI: 10.1021/jacs.2c02073
- Peng, X., Li, Y., Jiang, Z., Zhu, K., An, Q., Xiao, Z., Dong, X., and Zhai, S. (2024). "Photothermal-synergistic peroxymonosulfate activation promoting carbamazepine degradation by Porphyra-derived porous biochar composites: Performance, mechanism, transformation pathway and practical application," *Chemical Engineering Journal* 489, article 151263. DOI: 10.1016/j.cej.2024.151263
- Ravindiran, G., Rajamanickam, S., Janardhan, G., Hayder, G., Alagumalai, A., Mahian, O., Lam, S. S., and Sonne, C. (2024). "Production and modifications of biochar to engineered materials and its application for environmental sustainability: A review," *Biochar* 6, article 62. DOI: 10.1007/s42773-024-00350-1
- Repon, M. R., Dev, B., Rahman, M. A., Jurkonienė, S., Haji, A., Alim, M. A., and Kumpikaitė, E. (2024). "Textile dyeing using natural mordants and dyes: A review," *Environmental Chemistry Letters* 22, 1473-1520. DOI: 10.1007/s10311-024-01716-4
- Rojas, S., and Horcajada, P. (2020). "Metal-organic frameworks for the removal of emerging organic contaminants in water," *Chemical Reviews* 120, article 8378-8415. DOI: 10.1021/acs.chemrev.9b00797
- Saddique, Z., Imran, M., Javaid, A., Latif, S., Hussain, N., Kowal, P., and Boczkaj, G. (2023). "Band engineering of BiOBr based materials for photocatalytic wastewater treatment via advanced oxidation processes (AOPs) A review," *Water Resources and Industry* 29, article 100211. DOI: 10.1016/j.wri.2023.100211
- Senasu, T., Nijpanich, S., Juabrum, S., Chanlek, N., and Nanan, S. (2021). "CdS/BiOBr heterojunction photocatalyst with high performance for solar-light-driven degradation of ciprofloxacin and norfloxacin antibiotics," *Applied Surface Science* 567, article 150850. DOI: 10.1016/j.apsusc.2021.150850

- Sun, L., Gong, Y., Li, D., and Pan, C. (2022). "Biomass-derived porous carbon materials: Synthesis, designing, and applications for supercapacitors," *Green Chemistry* 24, article 3864-3894. DOI: 10.1039/d2gc00099g
- Suzuki, T., Hidaka, T., Kumagai, Y., and Yamamoto, M. (2020). "Environmental pollutants and the immune response," *Nature Immunology* 21, article 1486-1495. DOI: 10.1038/s41590-020-0802-6
- Wang, C., Feng, X., Shang, S., Liu, H., Song, Z., and Zhang, H. (2023a). "Adsorption of methyl orange from aqueous solution with lignin-modified metal-organic frameworks: Selective adsorption and high adsorption capacity," *Bioresource Technology* 388, article 129781. DOI: 10.1016/j.biortech.2023.129781
- Wang, H., Duan, R., Ding, L., Tian, L., Liu, Y., Zhang, Y., and Xu, R. (2023b). "Magnetic hydrochar derived from waste lignin for thallium removal from wastewater: Performance and mechanisms," *Bioresource Technology* 374, article 128736. DOI: 10.1016/j.biortech.2023.128736
- Wang, X., Li, Z., Xing, S., Kuang, W., Dong, C., and Liu, Y. (2023c). "Toward multitasking solar desalination: A Janus and scalable paper evaporator with light trapping, heat confinement, salt resistance, and pollutant degradation," *Journal of Materials Chemistry A* 11, article 10287-10296. DOI: 10.1039/d2ta09653f
- Wang, Z., Dou, M., Liu, X., Kang, S., Kong, L., Yang, H., Zhang, Y., Chen, Y., Zhu, H., and Dou, J. (2024). "Ternary Z-scheme α-Fe₂O₃/BiOBr/g-C₃N₄ photocatalyst for highly efficient hydrogen production coupled with diverse antibiotic degradation," *Journal of Environmental Chemical Engineering* 12, article 113080. DOI: 10.1016/j.jece.2024.113080
- Wei, B., Zhang, D., Jeyakumar, P., Trakal, L., Wang, H., Sun, K., Wei, Y., Zhang, X., Ling, H., He, S., Wu, H., Huang, Z., Li, C., and Wang, Z. (2024). "Iron-modified biochar effectively mitigates arsenic-cadmium pollution in paddy fields: A meta-analysis," *Journal of Hazardous Materials* 469, article 133866. DOI: 10.1016/j.jhazmat.2024.133866
- Wen, C., Li, D., Zhong, J., Wang, Z., Huang, S., Liu, H., Wu, J., Chen, P., Lv, W., and Liu, G. (2022). "*In situ* synthesis of S-scheme AgBr/BiOBr for efficient degradation of sulfonamide antibiotics: Synergistic effects of oxygen vacancies and heterojunctions promote exciton dissociation," *Chemical Engineering Journal* 450, article 138075. DOI: 10.1016/j.cej.2022.138075
- Wu, C., Zuo, H., Zhang, S., Zhao, S., Du, H., and Yan, Q. (2022). "A novel strategy to construct a direct Z-Scheme Bi@Bi₂O₂CO₃/g-C₃N₄ heterojunction catalyst via PDA electronic bridge," *Separation and Purification Technology* 294, article 121242. DOI: 10.1016/j.seppur.2022.121242
- Wu, M., Zhang, B., Wang, H., Chen, Y., Fan, M., Dong, L., Li, B., and Chen, G. (2024). "Exposed {1 1 0} facets of BiOBr anchored to marigold-like MnCo₂O₄ with abundant interfacial electron transfer bridges and efficient activation of peroxymonosulfate," *Journal of Colloid and Interface Science* 653, article 867-878. DOI: 10.1016/j.jcis.2023.09.106
- Xiao, F., Wang, Z., Fan, J., Majima, T., Zhao, H., and Zhao, G. (2021). "Selective electrocatalytic reduction of oxygen to hydroxyl radicals via 3-electron pathway with FeCo alloy encapsulated carbon aerogel for fast and complete removing pollutants," *Angewandte Chemie International Edition* 60, article 10375-10383. DOI: 10.1002/anie.202101804
- Xu, L., Wu, X. Q., Li, C. Y., Liu, N. P., An, H. L., Ju, W. T., Lu, W., Liu, B., Wang, X. F.,

- Wang, Y., and Wang, X. (2023). "Sonocatalytic degradation of tetracycline by BiOBr/FeWO₄ nanomaterials and enhancement of sonocatalytic effect," *Journal of Cleaner Production* 394, article 136275. DOI: 10.1016/j.jclepro.2023.136275
- Yang, Q., Qin, W., Xie, Y., Zong, K., Guo, Y., Song, Z., Luo, G., Raza, W., Hussain, A., Ling, Y., Luo, J., Zhang, W., Ye, H., and Zhao, J. (2022). "Constructing 2D/1D heterostructural BiOBr/CdS composites to promote CO₂ photoreduction," *Separation and Purification Technology* 298, article 121603. DOI: 10.1016/j.seppur.2022.121603
- Zhang, T., Qu, J., Wu, J., Jiao, F. Z., Li, C., Gao, F. L., Liu, J., Yu, Z. Z., and Li, X. (2024a). "All-in-one self-floating wood-based solar-thermal evaporators for simultaneous solar steam generation and catalytic degradation," *Advanced Functional Materials* 34, article 2403505. DOI: 10.1002/adfm.202403505
- Zhang, X., Hou, J., Zhang, S., Cai, T., Liu, S., Hu, W., and Zhang, Q. (2024b). "Standardization and micromechanistic study of tetracycline adsorption by biochar," *Biochar* 6, article 12. DOI: 10.1007/s42773-023-00299-7
- Zhang, Y., Cao, P., Zhu, X., Li, B., He, Y., Song, P., and Wang, R. (2021). "Facile construction of BiOBr ultra-thin nano-roundels for dramatically enhancing photocatalytic activity," *Journal of Environmental Management* 299, article 113636. DOI: 10.1016/j.jenvman.2021.113636
- Zhao, J., Chen, J., Chen, Z., Zhang, Y., Xia, D., and Wang, Q. (2020). "Flexible cotton fabrics/PDA/BiOBr composite photocatalyst using bioinspired polydopamine as electron transfer mediators for dye degradation and Cr(VI) reduction under visible light," *Colloids and Surfaces A: Physicochemical and Engineering Aspects* 593, article 124623. DOI: 10.1016/j.colsurfa.2020.124623
- Zhou, Y., Leong, S. Y., and Li, Q. (2023). "Modified biochar for removal of antibiotics and antibiotic resistance genes in the aqueous environment: A review," *Journal of Water Process Engineering* 55, article 104222. DOI: 10.1016/j.jwpe.2023.104222
- Zhu, Y., Wang, X., Li, Z., Fan, Y., Zhang, X., Chen, J., Zhang, Y., Dong, C., and Zhu, Y. (2021). "Husbandry waste derived coralline-like composite biomass material for efficient heavy metal ions removal," *Bioresource Technology* 337, article 125408. DOI: 10.1016/j.biortech.2021.125408
- Zhu, Y., Zhang, H., Ding, S., Ren, H., and Zhai, H. (2024). "Cellulose paper-based material: An efficient strategy of adjustable adsorption and enriched photodegradation toward multitasking environment remediation," *Separation and Purification Technology* 330, article 125365. DOI: 10.1016/j.seppur.2023.125365
- Zhu, Y., Zhang, H., Fu, P., Qin, L., Fu, Y., Zhang, J., Ren, H., and Zhai, H. (2025). "Integrated fiber paper-based composites enabling photo-Fenton synergistic degradation and switchable adsorption for efficient and multitasking pollutants removal," *Separation and Purification Technology* 355, article 129706. DOI: 10.1016/j.seppur.2024.129706

Article submitted: February 12, 2025; Peer review completed: March 29, 2025; Revisions accepted: May 23, 2025; Published: June 17, 2025.

DOI: 10.15376/biores.20.3.6218-6241

APPENDIX

SUPPORTING INFORMATION

S2.1 Characterization

Fourier Transform Infrared Spectra (FTIR, VERTEX 80V), X-ray photoelectron spectroscopy (XPS, AXIS UltraDLD), X-ray diffraction (XRD, Ultima IV) and scanning electron microscope (SEM, Regulus 8100) were used to characterize the chemical structure and surface morphology of the materials. Specific surface area analyzer (ASAP2020 HD88) was applied for testing the BET surface area. The photochemical and electrochemical properties of samples were investigated by using UV-vis spectrophotometer (Lambda 950), photoluminescence spectrometer (PL, Fluoromax+) and electrochemical workstation (CHI 760E).

S2.2 Electrochemical Properties Test

The electrochemical properties of the prepared photocatalytic materials were tested by an electrochemical workstation (CHI 760E). The experiment was conduct through setting up a traditional three-electrode system. The catalyst mixed solution was prepared by ultrasonic mixing of 5 mg catalyst powder, 2 mL anhydrous ethanol and 0.01 mL Nafion solution. By smearing the above solution on the FTO conductive glass, the working electrode was obtained after drying. Besides, Ag/AgCl electrode and Pt electrode were used as reference electrode and counter electrode, respectively. The lighting was provided by 300 W xenon lamps. And the electrolyte was 50 mmol/L Na2SO4 solution.

S2.3 Radical Species (RSs) Trapping Experiments

By adding different scavengers into degradation processes, the RSs trapping experiments were carried out. Each experiment was performed at the same condition as the photodegradation experiment. Among them, isopropanol (IPA), EDTA-2Na and 1,4-benzoquinone (BQ) were used to capture the \cdot OH, holes and \cdot O₂⁻ radicals, respectively.

S2.4 Band Distribution

The conduction band (CB) and valence band (VB) potentials of BiOBr can be estimated (Eq. 1 and 2):

$$E_{\rm VB} = X - E_{\rm e} + 0.5E_{\rm g}$$
 (1)

$$E_{\rm CB} = E_{\rm VB} - E_{\rm g} \tag{2}$$

where X is the electronegativity of BiOBr (6.17 eV), and E_e represents the free electron energy in hydrogen scale (4.5 eV). The calculated E_{VB} and E_{CB} of BiOBr were 3.01 eV and 0.33 eV respectively. In addition, PDA showed similar VB and CB (HOMO and LUMO), which was calculated as 1.30 eV and -1.4 eV, respectively.

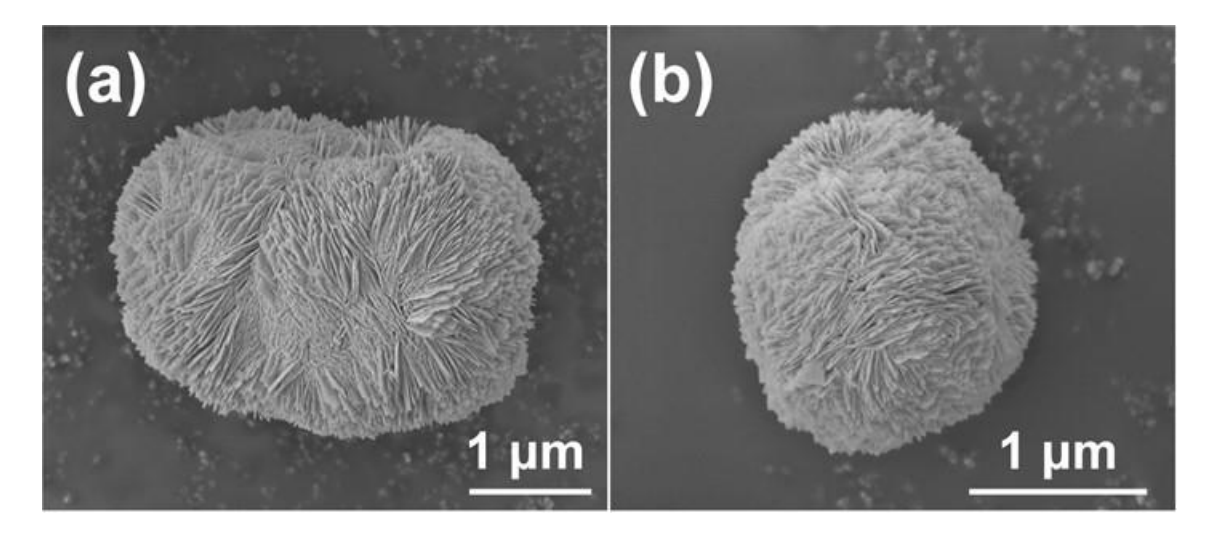


Fig. S1. SEM images of pure BiOBr

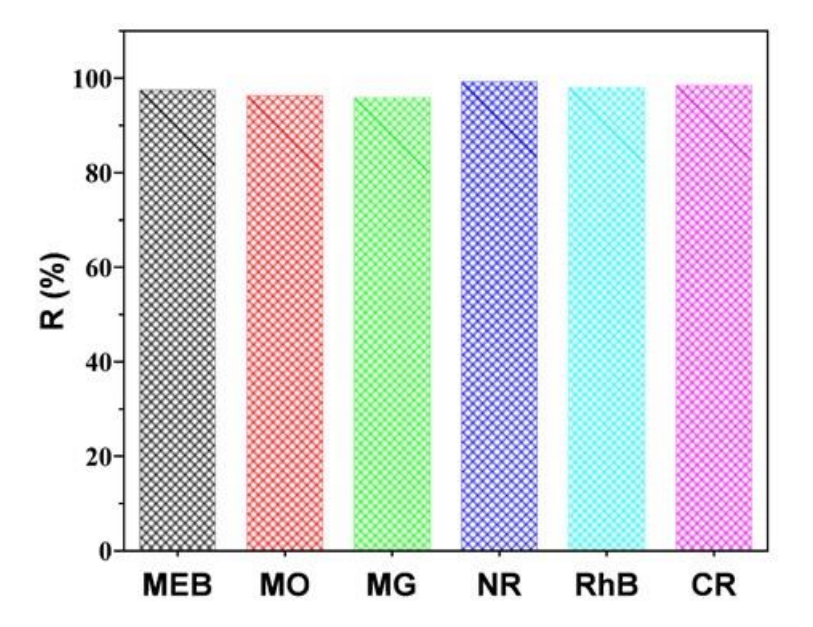


Fig. S2. The degradation efficiency of BiOBr/PSBM for various organic dyes

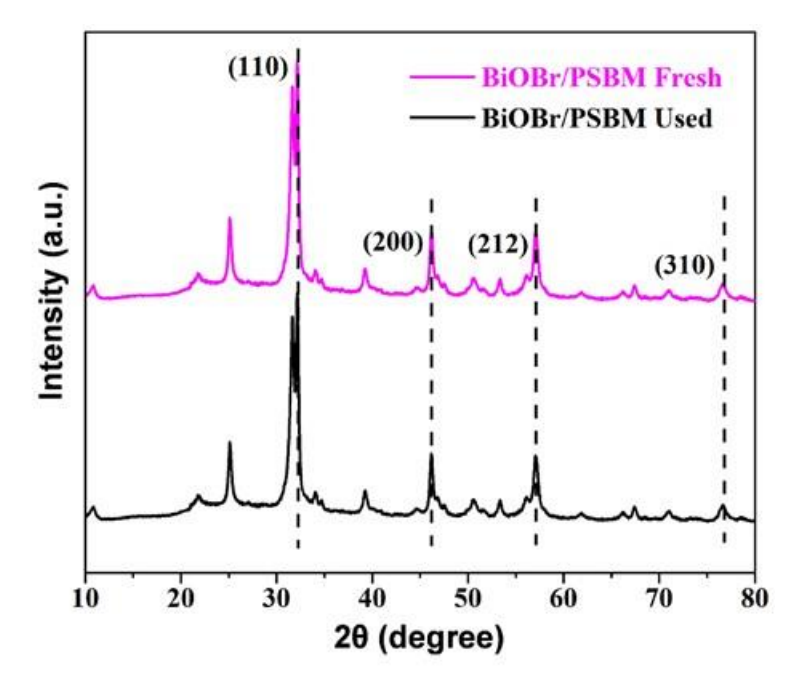


Fig. S3. XRD patterns of BiOBr/PSBM before and after using

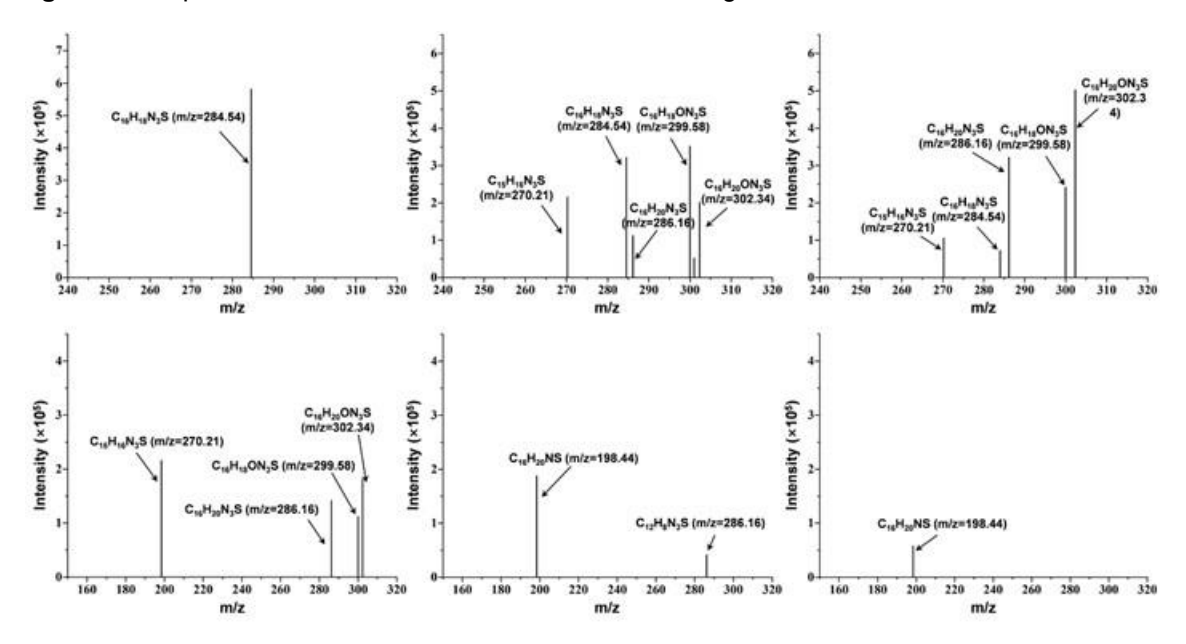


Fig. S4. The HPLC-MS of MEB solutions with different degradation times: (a) 0 min, (b) 10 min, (c) 20 min, (d) 30 min, (e) 40 min and (f) 50 min

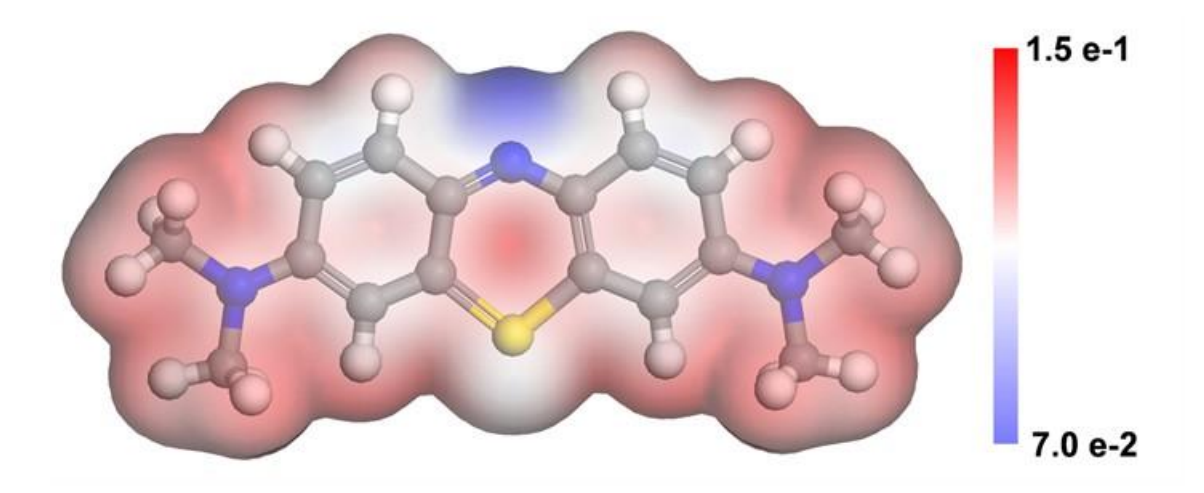


Fig. S5. Electrostatic potential distribution of MEB molecule

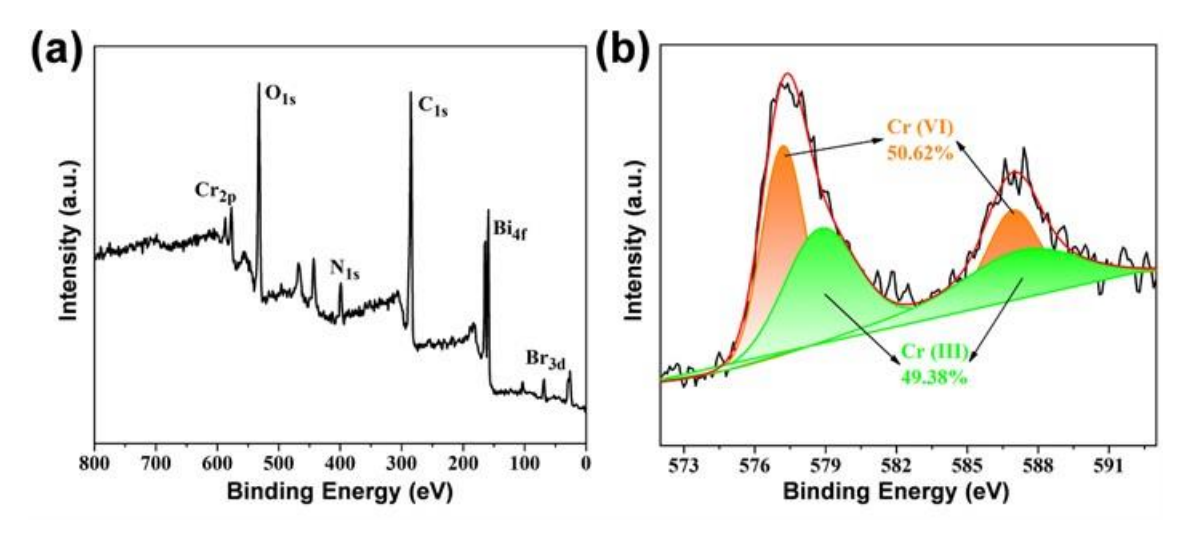


Fig. S6 (a) The XPS spectra of used BiOBr/PSBM and (b) Cr 2p spectra

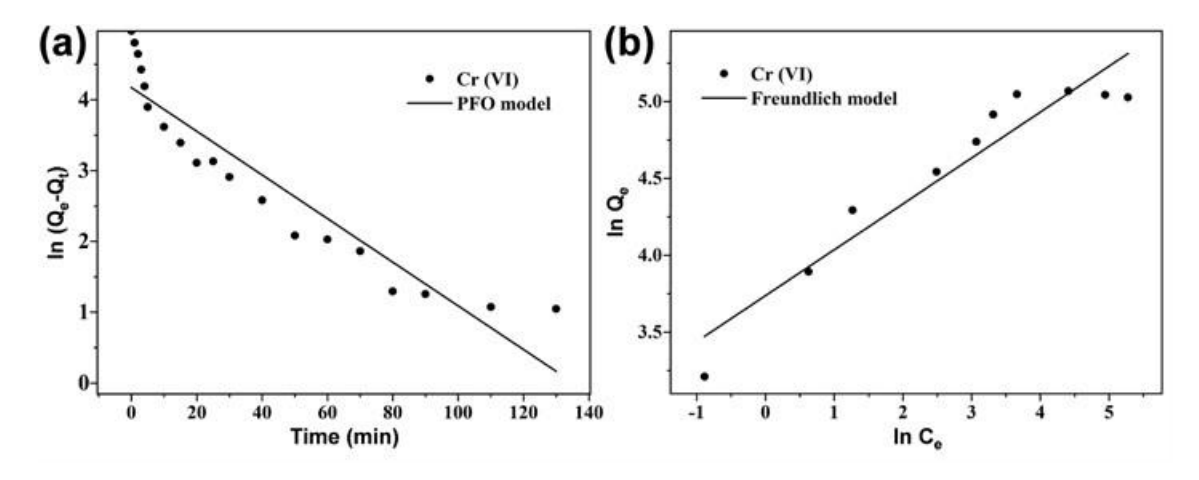


Fig. S7. (a) Adsorption kinetic fitting plots of Cr (VI) on BiOBr/PSBM by using PFO model. (b) Adsorption isothermal fitting plots of Cr (VI) on BiOBr/PSBM by using Freundlich model.